catalysts

MDPI

Article

A Facile Synthesis of Visible-Light Driven Rod-on-Rod like α-FeOOH/α-$AgVO_3$ Nanocomposite as Greatly Enhanced Photocatalyst for Degradation of Rhodamine B

Meng Sun, Raja Arumugam Senthil, Junqing Pan *, Sedahmed Osman and Abrar Khan

State Key Laboratory of Chemical Resource Engineering, Beijing Advanced Innovation Center for Soft Matter Science and Engineering, Beijing Engineering Center for Hierarchical Catalysts, Beijing University of Chemical Technology, Beijing 100029, China; 2015210392@grad.buct.edu.cn (M.S.); senthil2551988@gmail.com (R.A.S.); aboalseed87@hotmail.com (S.O.); abrarkhn89@yahoo.com (A.K.)

* Correspondence: jqpan@mail.buct.edu.cn; Tel./Fax: +86-10-64448461

Received: 22 August 2018; Accepted: 7 September 2018; Published: 12 September 2018

Abstract: In this work, we have synthesized the rod-on-rod–like α-FeOOH/α-$AgVO_3$ nanocomposite photocatalysts with the different amounts of solvothermally synthesized α-FeOOH nanorods via a simple co-precipitation method. The as-synthesized photocatalysts were characterized by X-ray diffraction (XRD), Fourier-transform infrared (FT-IR) spectroscopy, UV−Visible diffuse reflectance spectroscopy, scanning electron microscopy (SEM), element mapping, high-resolution transmission electron microscopy (HR-TEM) and X-ray photoelectron spectroscopy (XPS) analysis. The observed SEM images show that both α-$AgVO_3$ and α-FeOOH exhibits the rod-shaped morphology with nano size. Furthermore, the photocatalytic activities of the obtained photocatalysts were evaluated towards the degradation of Rhodamine B (RhB) under visible-light irradiation. It is demonstrated that the 3 mg α-FeOOH added to the α-FeOOH/α-$AgVO_3$ nanocomposite exhibited an enhanced photocatalytic performance as compared with the pure α-$AgVO_3$ and α-FeOOH. This significant improvement can be attributed to the increased photo-excited electron-hole pair separation efficiency, large portion of visible-light absorption ability and the reduced recombination of the electron-hole pair. The recycling test revealed that the optimized nanocomposite exhibited good photostability and reusability properties. In addition, the believable photodegradation mechanism of RhB using α-FeOOH/α-$AgVO_3$ nanocomposite is proposed. Hence, the developed α-FeOOH/α-$AgVO_3$ nanocomposite is a promising material for the degradation of organic pollutants in an aqueous environment.

Keywords: nanocomposite; co-precipitation method; photodegradation; rhodamine B; visible-light

1. Introduction

Well cleaned water is one of the most important factors for human life. The Earth is covered by around 70% water; however, only 2.5% of water is accessible for drinking, agriculture and other industrial consumption [1–3]. Currently, environmental protection and remediation are a tremendous threat to the world owing to the increased industrialization, environmental pollution and global warming [4,5]. Currently, large amounts of pollutants from synthetic organic dyes are easily mixed with the aquatic environment due to the rapid development of various industrial sectors such as textiles, dyeing and printing industries. Generally, this colored waste-water contains large numbers of organic compounds which are very toxic to human health as well as microorganisms [6,7]. In order to resolve these issues, it is a very necessary action to eradicate these organic pollutants from wastewater.

Several techniques such as adsorption [8], sonolysis [9], oxidation [10], (photo)-Fenton process [11], photocatalytic degradation [12,13] and ozonation [14] have been adapted for the eradication of organic effluents from waste-water. Among them, the semiconductor-based photocatalysis technique has received considerable attention owing to its low-cost, high photostability and eco-friendly nature towards the photocatalytic degradation of organic pollutants via freely available solar energy [15–17]. In addition, it can degrade the hazardous organic pollutants into nontoxic molecules such as CO_2, H_2O and mineral acids without creating secondary pollution and hence, the photocatalysis has been called green technology in recent times [18].

In general, the transition metal oxide-based semiconductor materials are recognized as sustainable and prospective photocatalysts for the removal of organic pollutants in wastewater [19–21]. Among the different metal oxides, the TiO_2 is the most frequently used photocatalyst for environmental remediation due to its outstanding properties of low cost, non-toxicity, high stability and relatively suitable band gaps for photocatalytic reaction [22,23]. However, the practical application of TiO_2 photocatalyst has been restricted so far in visible-light irradiation because of its limited response to solar light spectrum and fast recombination of electron-hole charge carriers for the large band-gap of 3.2 eV [24]. Therefore, the design and development of highly visible-light responsive semiconductor-based photocatalysts is an urgent requirement for its practical applications.

More recently, silver-based metal oxides such as Ag_2WO_4 [25,26], Ag_3PO_4 [27,28], Ag_3VO_4 [29], $AgVO_3$ [30], Ag_2MoO_4 [31] and Ag_2CrO_4 [32,33] have gained extensive consideration because they have shown an excellent photocatalytic activity in visible-light irradiation. Among them, $AgVO_3$ is widely reported as an emerging photocatalyst for degradation of the visible-light organic pollutants in waste-water due to its unique properties such as strong absorption in the visible light range, simple preparation, non-toxicity, high electrical conductivity and good crystallinity [34,35]. Besides, $AgVO_3$ has relatively good photostability like typical vanadium oxide compounds due to its narrow bandgap of less than 2.5 eV, displaying a superior photocatalytic activity in visible-light [36,37]. Unexpectedly, the photocatalytic activity of pure $AgVO_3$ is still limited due to its low separation efficiency and rapid recombination of photo-excited electron-hole pairs as a result of narrow band gap energy [30]. To tackle this issue, it is essential to explore sufficient ways to further improve the separation efficiency of photo-excited charge carriers as well as photocatalytic performance. Over the past few decades, researchers have modified the $AgVO_3$ via preparation of heterojunction composite materials with other semiconductors which have suitable band potentials to reduce the recombination of charge carriers and hence, the photocatalytic activity has been improved. In addition, many $AgVO_3$-based composite photocatalysts, such as $AgCl/AgVO_3$ [38], $Ag_3PO_4/AgVO_3$ [39], $BiVO_4/AgVO_3$ [40,41], $MoS_2/AgVO_3$ [42], graphene/$AgVO_3$ [43], g-C_3N_4/Ag/$AgVO_3$ [44,45], $Ag_2CrO_4/AgVO_3$ [46] and $Ba_5Ta_4O_{15}/AgVO_3$ [47] have been reported to have the superior photocatalytic performance because of their increased electron-hole separation efficiency as compared with pure $AgVO_3$.

On the other hand, α-FeOOH is another important semiconductor material in the field of photocatalysts because of its extensive absorption band position in the visible light region, inexpensiveness, non-toxicity, and corrosion resistance [48–50]. Moreover, the α-FeOOH can easily couple with other semiconductors to enhance their photocatalytic performance in visible-light irradiation, thus obtaining the heterojunction photocatalysts [51,52]. A few attempts have been described on α-FeOOH-based composite photocatalyst for the degradation of organic pollutants from the aquatic environment. For example, Feng et al. [53] synthesized α-FeOOH/Ag_3PO_4 nanocomposites with higher photocatalytic activity towards elimination of Rhodamine B (RhB) solution in irradiation visible light than that for the pure Ag_3PO_4. Yang et al. [54] reported the α-FeOOH/g-C_3N_4 composite with superior photocatalytic ability for the elimination of organic pollutants such as RhB, Methylene Blue (MB) and Methyl Orange (MO) under visible-light irradiation. More recently, Malathi [52] et al. also prepared α-FeOOH/BiOI nanocomposites by a facile wet-chemical method, which greatly improved photocatalytic activity for the visible-light degradation of RhB as compared with pure BiOI. In addition, the α-FeOOH is an ideal material to couple with $AgVO_3$ to inhibit the recombination

of photo-excited electron-hole pairs through their well matched band gap positions, resulting in the overall expected properties to enhance its photocatalytic activity. Therefore, in the present study, the α-FeOOH was selected as co-catalyst to fabricate α-FeOOH/α-$AgVO_3$ nanocomposite photocatalysts via a facile co-prepetition method at room temperature. Also, to the best of our knowledge, the α-FeOOH/α-$AgVO_3$ nanocomposite has not yet been reported as a photocatalyst for environmental remediation in literatures.

Herein, we have synthesized well-uniform α-FeOOH nanorods using solvothermal method. Apart from that, a series of the rod-on-rod–like α-FeOOH/α-$AgVO_3$ nanocomposites were synthesized with different amounts of α-FeOOH by using a facile co-precipitation method at room temperature. The photocatalytic abilities of the as-syntheszied photocatalyts were assessed toward the discharging of RhB in waste-water under visible-light irradiation. The acquired degradation results revealed that the α-FeOOH/α-$AgVO_3$ nanocomposites were found to have the superior photocatalytic activity when compared with pure α-FeOOH and α-$AgVO_3$. Furthermore, the nanocomposite possesses an excellent photo-stability and reusability nature. Lastly, the possible charge-transfer mechanism for the increased degradation of RhB using α-FeOOH/α-$AgVO_3$ nanocomposites has also been proposed. Consequently, the present study shows that the α-FeOOH/α-$AgVO_3$ nanocomposite will be a promising candidate for waste-water treatment and other environmental remediation.

2. Results and Discussion

2.1. Schematic Representation of the Synthesis Process

Figure 1 shows the schematic representation of the synthesis process of α-FeOOH/α-$AgVO_3$ nanocomposite. First, the α-FeOOH was synthesized using a solvothermal method and it exhibited the nanorods-shaped morphology. Afterwards, the α-FeOOH/α-$AgVO_3$ nanocomposites were synthesized through a facile co-precipitation method at room temperature. The as-obtained material shows that the α-FeOOH nanorods are well deposited on the surface of α-$AgVO_3$ nanorods. This structure is beneficial to the synergistic effect between the α-FeOOH and α-$AgVO_3$. In addition, this nanocomposite exhibits the enhanced visible-light adsorption ability as compared with pure α-$AgVO_3$ which can support to increasing the photocatalytic degradation efficiency of RhB under visible-light illumination by reducing the recombination of photo-excited electron-hole pairs. Hence, the α-FeOOH/α-$AgVO_3$ can be recognized as a potential materials as photocatalyst for the removal of organic pollutants in wastewater.

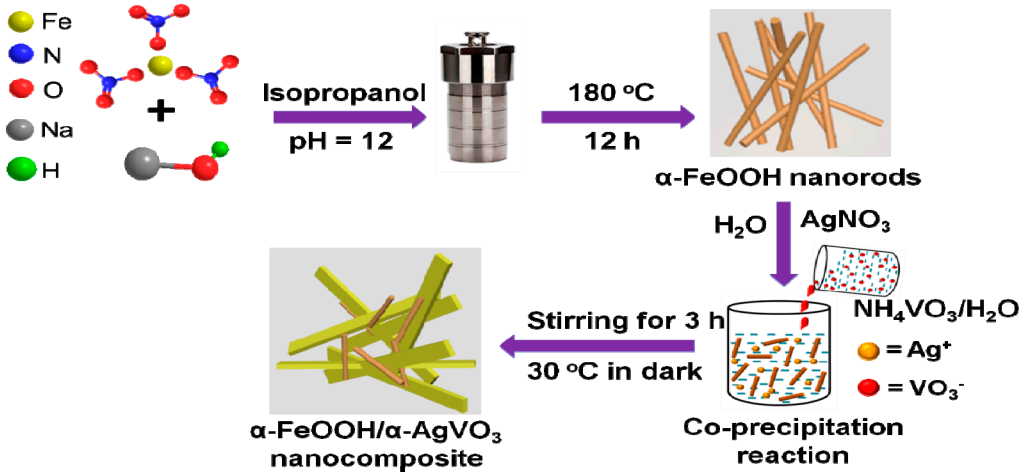

Figure 1. A schematic representation of the synthesis route of α-FeOOH/α-$AgVO_3$ nanocomposite photocatalyst.

2.2. Structural, Optical and Morphological Studies

The phase formation and purity of the as-synthesized photocatalysts were determined by X-ray diffraction (XRD) analysis. The XRD patterns of the pure α-FeOOH, pure α-$AgVO_3$ and different α-FeOOH/α-$AgVO_3$ nanocomposites are shown in Figure 2a,b. It is shown that the XRD peaks of pure α-FeOOH are well consistent with the orthorhombic structure of α-FeOOH (JCPDS card No. 81-0462) [52,53]. The XRD pattern of pure α-$AgVO_3$ is well indexed to the standard monoclinic structure of α-$AgVO_3$ (JCPDS card No. 89-4396) [41,55]. Additionally, the characteristic XRD peaks of the α-FeOOH were not found in the case of α-FeOOH/α-$AgVO_3$ nanocomposites due to the presence of a low amount of α-FeOOH content in the nanocomposites. However, there are no new peaks detected in the nanocomposite, indicating the high purity of the as-synthesized samples.

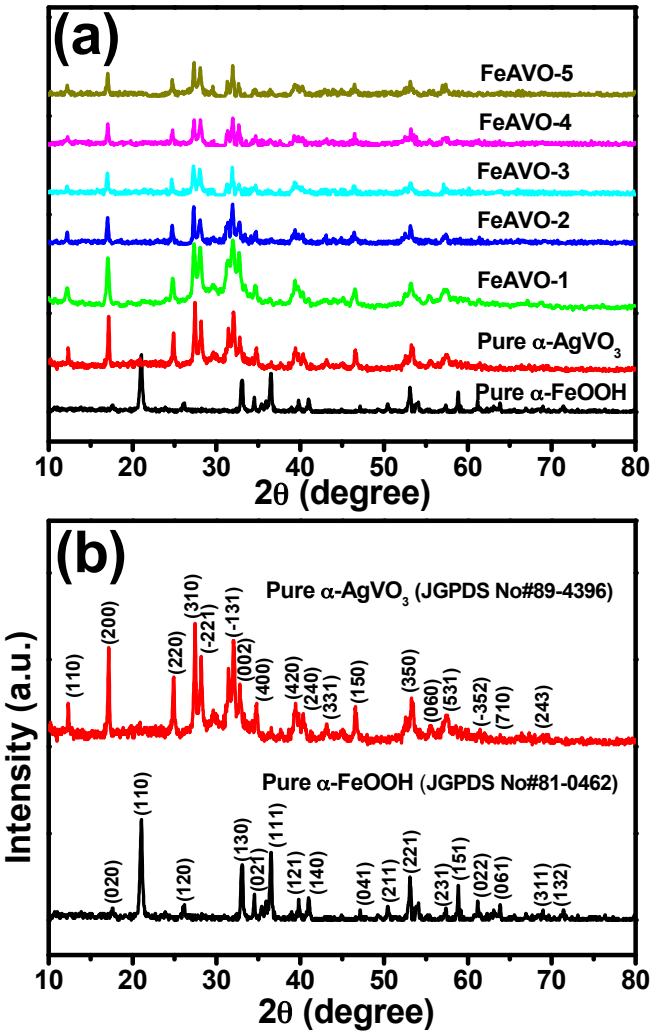

Figure 2. (**a**) X-ray diffraction (XRD) patterns of pure α-FeOOH, pure $AgVO_3$ and different α-FeOOH/α-$AgVO_3$ nanocomposite photocatalysts and (**b**) XRD patterns of pure α-FeOOH and pure α-$AgVO_3$ with their corresponding (hkl) values.

The FT-IR spectra of pure α-FeOOH, pure α-$AgVO_3$ and different α-FeOOH/α-$AgVO_3$ nanocomposites are presented in Figure 3a. The pure $AgVO_3$ exhibits the two absorption bands at 647 cm^{-1} and 928 cm^{-1} due to the symmetric stretching vibration of VO_3 and the bands appeared at 773 893 cm^{-1} and 893 cm^{-1}, which are related to the anti-symmetric stretching vibrations of VO_3 [37]. Also, the band located at 556 cm^{-1} is due to the symmetry stretching mode of V-O-V. The two broad absorption bands detected at 1633 cm^{-1} and 3429 cm^{-1} are attributed to the physical absorption of

water molecules on the surface of the $AgVO_3$ [56]. Additionally, the pure α-FeOOH shows the two vibrational bands at 893 cm^{-1} and 799 cm^{-1}, corresponding to the bending vibrations of the Fe-O-H bonds of α-FeOOH [52]. The absorption bands observed at 634 cm^{-1} and 497 cm^{-1} are related to the stretching vibration of the Fe-O bonds of α-FeOOH. A broad absorption band at 3138 cm^{-1} is due to the stretching vibration of the O-H group of α-FeOOH. However, in the case of α-FeOOH/$AgVO_3$ nanocomposites, the α-$AgVO_3$ peaks intensities are found to be decreased by the addition of α-FeOOH, which is due to the formation composites with α-FeOOH and also the merging of vibrational peaks of α-FeOOH and α-$AgVO_3$.

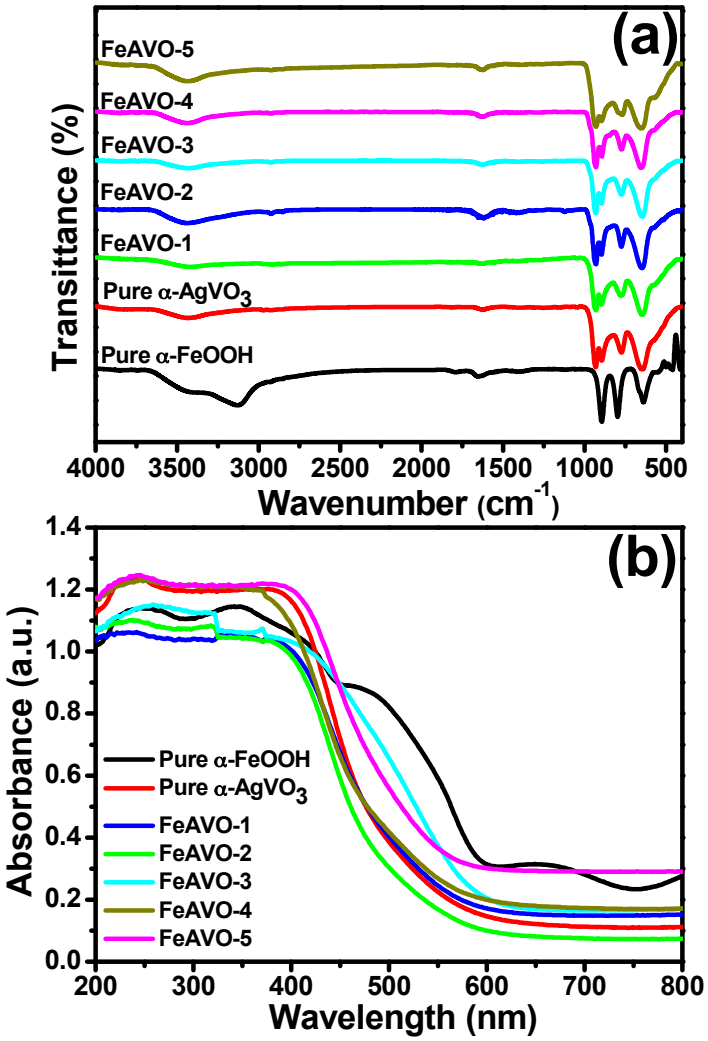

Figure 3. (**a**) Fourier-transform infrared (FT-IR) spectra of pure α-FeOOH, pure α-$AgVO_3$ and different α-FeOOH/α-$AgVO_3$ nanocomposite photocatalysts and (**b**) UV-Visible diffuse reflectance spectra of pure α-FeOOH and pure α-$AgVO_3$ and optimized FeAVO-3 nanocomposite photocatalysts.

The optical absorption nature of the fabricated photocatalysts was determined through UV-vis diffusion reflectance spectroscopy analysis and the obtained UV-vis diffuse reflectance spectra of pure α-FeOOH, pure α-$AgVO_3$ and FeAVO-3 nanocomposite photocatalysts are given in Figure 3b. As seen from Figure 3b, the absorption edges (λg) of pure α-FeOOH, pure α-$AgVO_3$, FeAVO-1, FeAVO-2, FeAVO-3, FeAVO-4 and FeAVO-5 nanocomposites are estimated to be around 645 nm, 557 nm, 526 nm, 564 nm, 622 nm, 602 nm and 584 nm, respectively. It can be seen that the absorption edges of FeAVO-3 nanocomposite are much higher than that of pure α-$AgVO_3$. That is owing to the slow recombination of photo-excited electrons and holes, which can assist the strong absorption in the visible light region to degrade more organic pollutants [17]. Furthermore, the band-gap energy (E_g) of the as-synthesized

photocatalysts can be calculated via the equation, $E_g = 1240/\lambda g$ (eV), where, λg is the absorption edge, which is obtained from the intercept between the tangent of the absorption curve and abscissa [57]. The E_g values of pure α-FeOOH, pure $AgVO_3$, FeAVO-1, FeAVO-2, FeAVO-3, FeAVO-4 and FeAVO-5 nanocomposites are calculated to be 1.92 eV, 2.22 eV, 2.35 eV, 2.19 eV, 1.99 eV, 2.05 eV and 2.12 eV, respectively. It is shown that FeAVO-3 nanocomposite has the much lower Eg value when compared with α-$AgVO_3$, indicating the higher absorption efficient light in the visible light region which may be favorable for its photocatalytic performance [28,31].

The SEM measurement was performed to explore the surface morphology of the as-synthesized photocatalysts. The SEM images of the pure α-FeOOH, pure α-$AgVO_3$ and the optimized FeAVO-3 nanocomposite photocatalysts at different magnifications are presented in Figure 4a–f. As seen from Figure 4a,b, the pure α-FeOOH exhibits a well uniform nanorod-shaped morphology. Meanwhile, the pure α-$AgVO_3$ also exhibited the nanorod-shaped morphology with some irregular shaped nanoparticles as shown in Figure 4c,d. From Figure 4e,f, the SEM images of FeAVO-3 nanocomposite show that the α-FeOOH nanorods are attached on the surface of the nanorod-shaped α-$AgVO_3$. This result confirms the formation of α-FeOOH/α-$AgVO_3$ nanocomposite material. Also, the existence of good interfacial contact between the α-FeOOH and α-$AgVO_3$ may facilitate reducing the hole-electron recombination and improving the photocatalytic activity of the nanocomposite. For further investigation of the surface morphology of the α-FeOOH/α-$AgVO_3$ nanocomposite photocatalyst, the HR-TEM analysis was carried out for the optimized FeAVO-3 nanocomposite photocatalyst. The HR-TEM images of FeAVO-3 nanocomposite at different magnifications with its corresponding selected area (electron) diffraction (SAED) pattern are shown in Figure 5a–d). Obviously, the HR-TEM images demonstrate that the α-FeOOH nanorods are well attached on the surface of α-$AgVO_3$ nanorods. This observed HR-TEM result is well consistent with the SEM analysis. In addition, the SAED pattern of FeAVO-3 nanocomposite contains proper crystalline structure of both α-FeOOH and α-$AgVO_3$, which clearly indicates the successful synthesis of α-FeOOH/α-$AgVO_3$ nanocomposite photocatalysts.

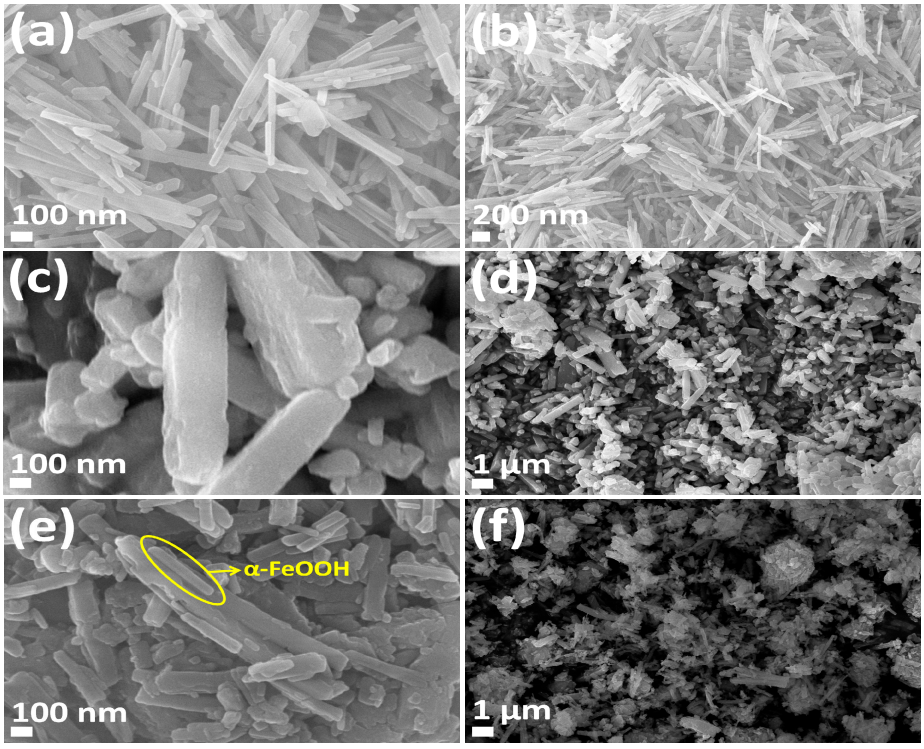

Figure 4. Scanning electron microscopy (SEM) images of (**a**,**b**) pure α-FeOOH, (**c**,**d**) pure α-$AgVO_3$ and (**e**,**f**) optimized FeAVO-3 nanocomposite photocatalysts at different magnification.

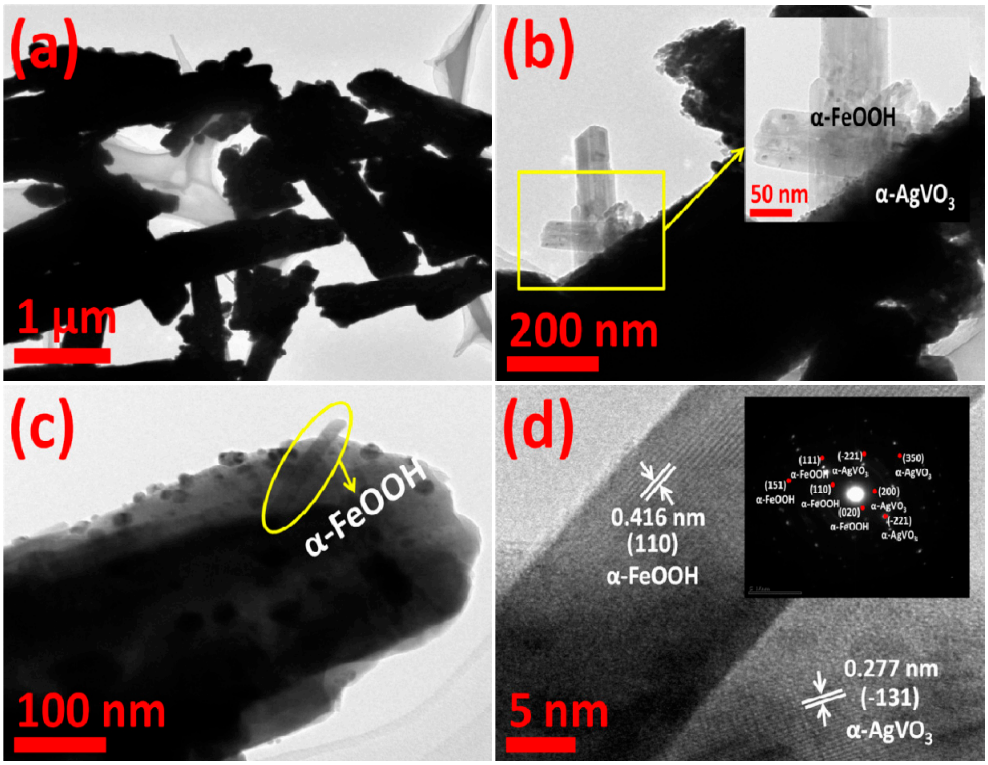

Figure 5. (**a**–**d**) High-resolution transmission electron microscopy (HR-TEM) images of the optimized FeAVO-3 nanocomposite photocatalyst at different magnifications with the corresponding selected area (electron) diffraction (SAED) pattern.

The elemental compositions of the as-synthesized nanocomposite were assessed from element mapping analysis. The typical element mapping images of the optimized FeAVO-3 nanocomposite are given in Figure 6. It is shown that the elements of Ag, V, Fe and O only appear for the as-synthesized nanocomposite, indicating the successful synthesis of α-FeOOH/α-$AgVO_3$ nanocomposite without any impurities. The XPS was also employed to extensively verify the chemical composition and the chemical states of the as-synthesized α-FeOOH/α-$AgVO_3$ nanocomposite. The XPS spectrum of the optimized FeAVO-3 nanocomposite photocatalyst: (a) Full survey spectrum, (b) Ag 3d, (c) V 2p, (d) O 1s and (d) Fe 3d are displayed in Figure 7. The high resolution XPS spectra in Figure 7a indicate the FeAVO-3 nanocomposite is composed of the elements of Ag, V, O, and Fe, which also prove the high purity of the synthesized samples. In Figure 7b, two XPS peaks of Ag 3d concentrate at 367.9 eV and 374.1 eV, corresponding to the Ag $3d_{5/2}$ and Ag $3d_{3/2}$ binding energies of Ag^{+}, respectively [46]. Also, the peaks were not observed at the binding energies of 369.2 eV and 375.8 eV, indicating no formation of Ag^{0} metal in the nanocomposite. The two XPS peaks appeared at 516.9 eV and 524.4 eV in Figure 7c which are assigned to the V $2P_{5/2}$ and V $2P_{3/2}$ binding energies of V^{5+}, respectively [30]. Whereas, in the case of O 1s, two XPS peaks detected in Figure 7e at 530.02 eV and 531.42 eV are attributed to the V-O bond in the $AgVO_3$ and the Fe-O bond in the α-FeOOH, respectively [43]. As shown in Figure 4f, the two XPS peaks are located at 711.5 eV and 719.5 eV due to the binding energies of Fe $2p_{3/2}$ and Fe $2p_{1/2}$, respectively, which indicates that the Fe^{3+} is present in the nanocomposite. The results confirm the successful formation of α-FeOOH/α-$AgVO_3$ composites.

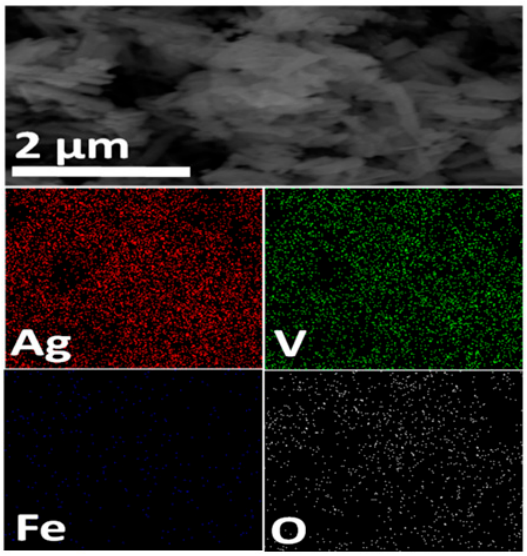

Figure 6. Element mapping images of the optimized FeAVO-3 nanocomposite photocatalyst.

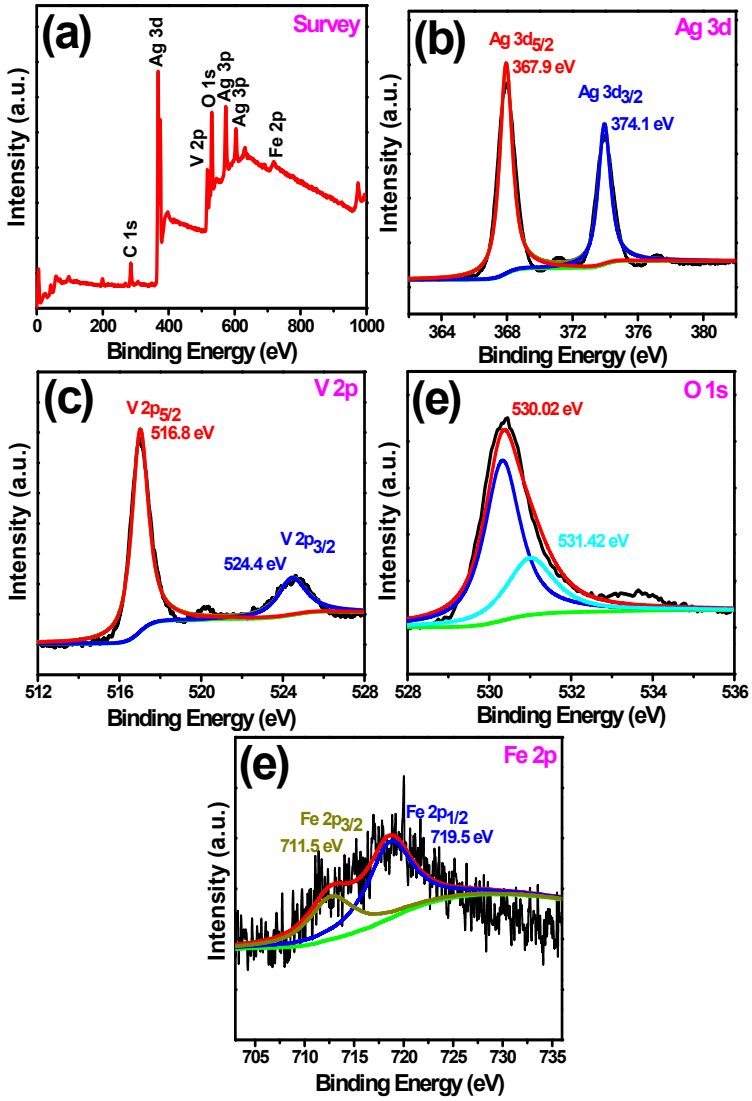

Figure 7. X-ray photoelectron spectra (XPS) of the optimized FeAVO-3 nanocomposite photocatalyst: (**a**) Full survey spectrum, (**b**) Ag 3d, (**c**) V 2p, (**d**) O 1s and (**e**) Fe 3d.

2.3. Photocatalytic Performance

The photocatalytic performances of the as-synthesized photocatalysts were assessed by the photodegradation of pollutant RhB under visible-light illumination. In order to find out the photostability nature of RhB in the visible-light region, the blank experiments were also performed without any photocatalysts for 90 min. The obtained degradation results of pure α-FeOOH, pure α-$AgVO_3$ and different α-FeOOH/α-$AgVO_3$ nanocomposite photocatalysts are presented in Figure 8a,b. From Figure 8a,b, it can be seen that the concentration of RhB is not changed after 90 min of blank experiments under illumination of visible-light, indicating that the RhB has almost no self-degradability. The pure α-FeOOH and pure α-$AgVO_3$ shows only 23.9% and 38.8% of degradation efficiency, respectively. Whereas, the α-FeOOH/α-$AgVO_3$ nanocomposites displayed the greatly enhanced photocatalytic performance when compared with pure α-FeOOH and pure α-$AgVO_3$. The improvement in the nanocomposite photocatalysts is mainly attributed to the lower band-gap energy and the extended visible-light absorption ability [32,33]. However, among the different nanocomposites, the FeAVO-3 nanocomposite achieves the highest degradation efficiency of 88.0% within 90 min, superior to the other nanocomposites. The decreased photocatalytic performance of the nanocomposites beyond the addition of 3 mg of α-FeOOH is probably ascribed to the poor catalytic activity of α-FeOOH, clearly indicating that the amount of α-FeOOH also creates the major impact on the photocatalytic performance of α-FeOOH/α-$AgVO_3$ nanocomposite.

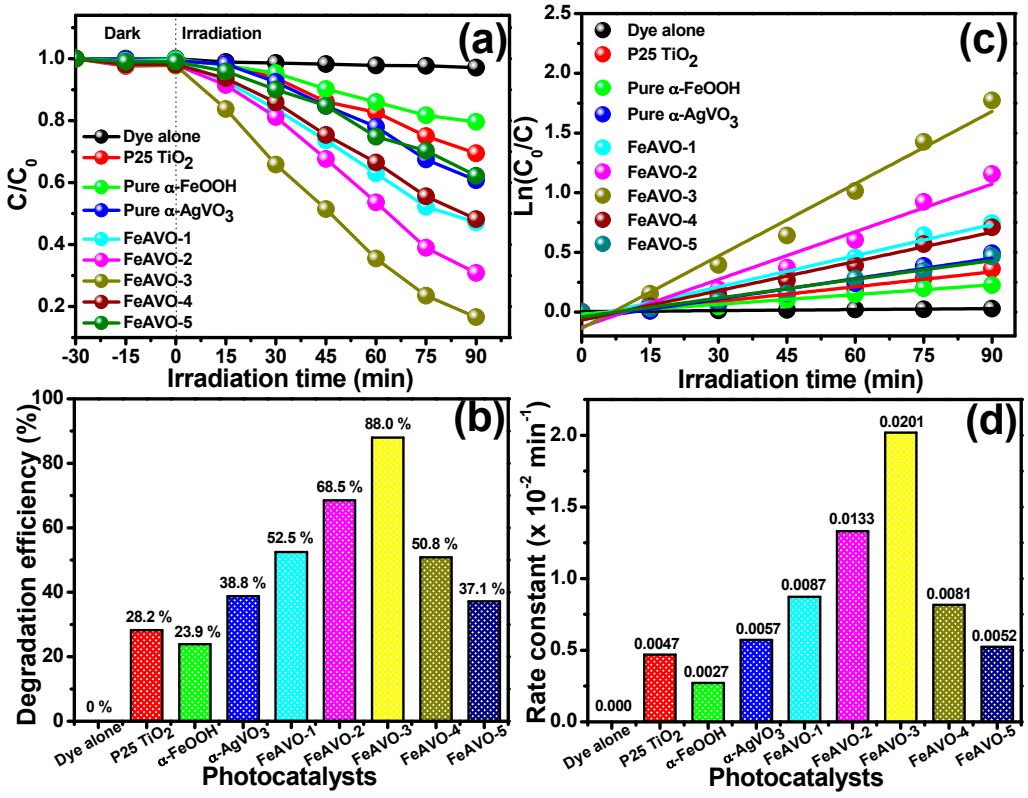

Figure 8. (**a**) Photodegradation plots, (**b**) the degradation efficiency, (**c**) first-order kinetics plots and (**d**) the rate constant values of the pure α-FeOOH, pure α-$AgVO_3$ and different α-FeOOH/α-$AgVO_3$ nanocomposite photocatalysts for the degradation of Rhodamine B (RhB) under visible-light illumination.

In addition, the obtained photodegradation results were fitted with the following first order kinetics Equation (1) to determine the degradation rate of the reaction.

$$\mathrm{Ln}(C_0/C) = kt \quad (1)$$

where, C_0 and C denote the RhB concentration at the initial stage and at a certain time, respectively, k denotes the pseudo-first-order rate constant (min^{-1}) and t denotes irradiation time (min). The linear relationship between $Ln(C_0/C)$ and t towards the degradation of RhB and the acquired rate constant values corresponding to different samples are illustrated in Figure 8c,d. It is clearly revealed that the RhB degradation follows the pseudo-first-order kinetics. As seen from Figure 8d, the FeAVO-3 nanocomposite exhibits the highest rate constant value when compared with other samples.

The optimized FeAVO-3 nanocomposite was used to investigate the influence of catalyst dosage on photodegradation of RhB. The photodegradation experiment was carried out by changing the catalyst amount from 0.25 g L^{-1} to 1.50 g L^{-1} under visible-light eradiation and the result is shown in Figure 9a. This shows that the RhB degradation is significantly increased with increasing the catalyst dosage from 0.25 g L^{-1} to 1.00 g L^{-1}. This improvement of degradation may be owing to the availability of the more active surface catalyst sites to adsorb a large number of dye molecules on the surface of the photocatalyst and to extend visible-light absorption, resulting in the increase of photocatalytic activity [52]. Even though, the decreased RhB degradation is observed beyond the addition of 1.00 g L^{-1}, that may be reason for the turbidity of solution and scattering of irradiated light [58]. Lastly, this result shows that the higher catalyst dosage is not appropriate for degradation of RhB.

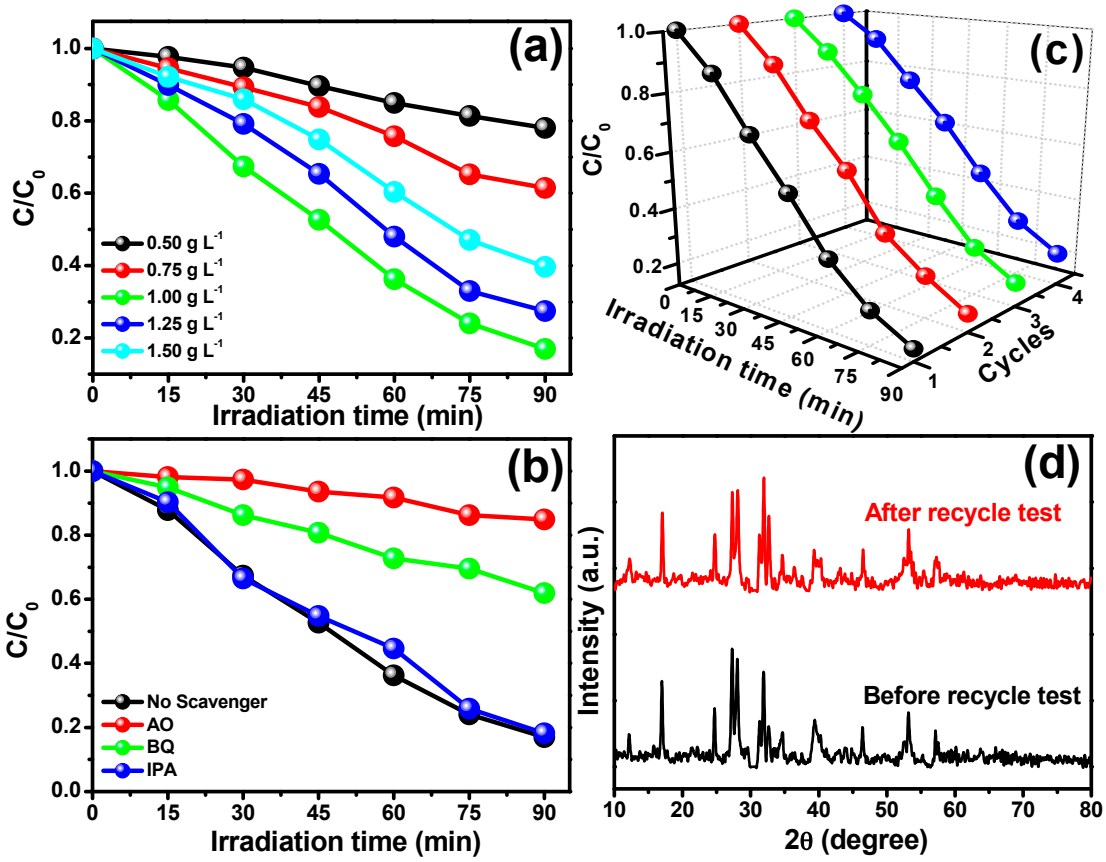

Figure 9. (**a**) Effect of catalyst dosage from 0.50 g L^{-1}–1.50 g L^{-1}, (**b**) effect of scavengers on the degradation of RhB, (**c**) the recycling runs for the degradation of RhB using the optimized FeAVO-3 nanocomposite in visible-light irradiation and (**d**) XRD patterns of the optimized FeAVO-3 nanocomposite before and after recycling test.

The active species which are more responsible for the degradation process of RhB by FeAVO-3 nanocomposite is also another important factor for its practical application. Hence, the different types of radical scavengers specifically benzoquinone (BQ), ammonium oxalate (AO) and isopropanol (IPA) were introduced into the reaction solution as scavengers of superoxide radical ($\bullet O_2^-$), hole (h^+) and

hydroxide radical (•OH), respectively, for carrying out radical trapping measurements as given in Figure 9b. As shown in Figure 9b, no considerable change is observed in the degradation of RhB with the addition of IPA, indicating non-participation of •OH in the degradation process. In addition, the obvious decrease in the degradation of RhB is observed when introducing AO and BQ into the reaction solution. This result reveals that the h^+ and $\bullet O_2^-$ are important active species and play an essential role in the degradation process of RhB over α-FeOOH/α-$AgVO_3$ nanocomposite under visible-light excitation.

The excellent photostability and reusable nature of the as-synthesized photocatalysts are the most crucial factors for its large-scale applications. Therefore, the four successive recycling experiments were performed for the optimized FeAVO-3 nanocomposite under visible-light illumination as depicted in Figure 9c. At the end of every cycle, around 70% of the photocatalyst sample was recovered from the degraded solution via centrifugation followed by being dried at 80 °C for 3 h. After that, the recovered samples were weighed again and followed by replenishing the lost portion and introduced into fresh RhB solution for the next batch. Figure 9c reveals that the photocatalytic activity of the FeAVO-3 nanocomposite remains constant after four cycles. Moreover, the changes in the crystalline structure of the FeAVO-3 nanocomposite were analyzed by XRD before and after recycling experiments and the acquired XRD patterns are given in Figure 9d. It is indicated that there is no considerable change in the crystalline structure of the sample before and after recycling. These observed results infer that the α-FeOOH/α-$AgVO_3$ nanocomposite exhibits excellent photostability and reusability properties. Consequently, the as-synthesized α-FeOOH/α-$AgVO_3$ nanocomposite is a potential material and can be used in long-term practical application for the removal of organic pollutants from waste-water. Additionally, the comparison of photocatalytic performance of the as-synthesized α-FeOOH/α-$AgVO_3$ nanocomposite towards the degradation of RhB with that of some previously reported silver-based photocatalysts and commercially available P25 TiO_2 nanoparticles is shown in Table 1. It is revealed that the α-FeOOH/α-$AgVO_3$ nanocomposite exhibits a superior photocatalytic activity to those previously reported in the literatures and P25 TiO_2 [30,31,41,53,59,60].

Table 1. Comparison of photocatalytic activity of the α-FeOOH/α-$AgVO_3$ nanocomposite with that of other silver-based composite materials in the literatures.

Material	Pollutant	Light Source	Irradiation Time	Degradation Efficiency (%)	Reference
$InVO_4/AgVO_3$	RhB	Visible	200 min	99.8	[30]
g-C_3N_4/Ag_2MoO_4	RhB	Visible	120 min	85.0	[31]
$BiVO_4/AgVO_3$	RhB	Visible	240 min	65.7	[41]
α-FeOOH/Ag_3PO_4	RhB	Visible	120 min	76.0	[53]
Ag_3VO4/ZnO	RhB	Visible	450 min	100	[59]
Ag_2WO_4/WO_3	RhB	Visible	120 min	94.0	[60]
P25 TiO_2	RhB	Visible	90 min	28.2	This work
α-FeOOH/α-$AgVO_3$	RhB	Visible	90 min	88.0	This work

2.4. Photocatalytic Degradation Mechanism

A predictable charge-transfer mechanism for the increased degradation of RhB using α-FeOOH/α-$AgVO_3$ nanocomposite under irradiation of visible-light is presented in Figure 10. The different energy levels are the most important requirement for formation of the composites of two different photocatalysts, which helped to produce higher electron-hole charge carriers through reducing the recombination. The valence band (VB) and conduction band (CB) potentials of the as-obtained pure α-FeOOH and α-$AgVO_3$ were determined through the following Equations (2) and (3) [24,61].

$$E_{VB} = X - E^e + 0.5E_g \quad (2)$$

$$E_{CB} = E_{VB} - E_g \quad (3)$$

Here, E_{VB} is the VB potential, E_{CB} is the CB potential, X is the electronegativity and E_g is the band-gap energy of the semiconductor, respectively. E^e stands for the energy of free electrons on the hydrogen scale (−4.5 eV). Furthermore, the absolute electronegativity values of α-FeOOH and $AgVO_3$ are 6.38 eV and 5.86 eV, respectively [45,52]. According to the above equations, the VB and CB potential values of the pure α-$AgVO_3$ are calculated to be 2.47 eV and 0.24 eV, respectively. In parallel, the VB and CB potential values of pure α-FeOOH are calculated to be 2.84 eV and 0.92 eV, respectively, and these calculated values are also shown in Figure 10. Under illumination, the ground states of α-$AgVO_3$ and α-FeOOH photocatalysts are turned into excited states, creating photo-excited electron-hole pairs. Afterwards, the photo-excited electron in the CB of α-$AgVO_3$ can freely transfer into that in the CB of α-FeOOH because the CB potential of α-$AgVO_3$ is lower than that of the α-FeOOH. Simultaneously, the photo-excited hole in the VB of α-FeOOH can readily transfer into that in the VB of α-$AgVO_3$ because the VB potential of α-FeOOH is higher than that of the α-$AgVO_3$. In this manner, the electron and holes are efficiently separated as a result of inhibition of the electron-hole recombination, which is beneficial for the improvement of photocatalytic performance of the α-FeOOH/α-$AgVO_3$ nanocomposite.

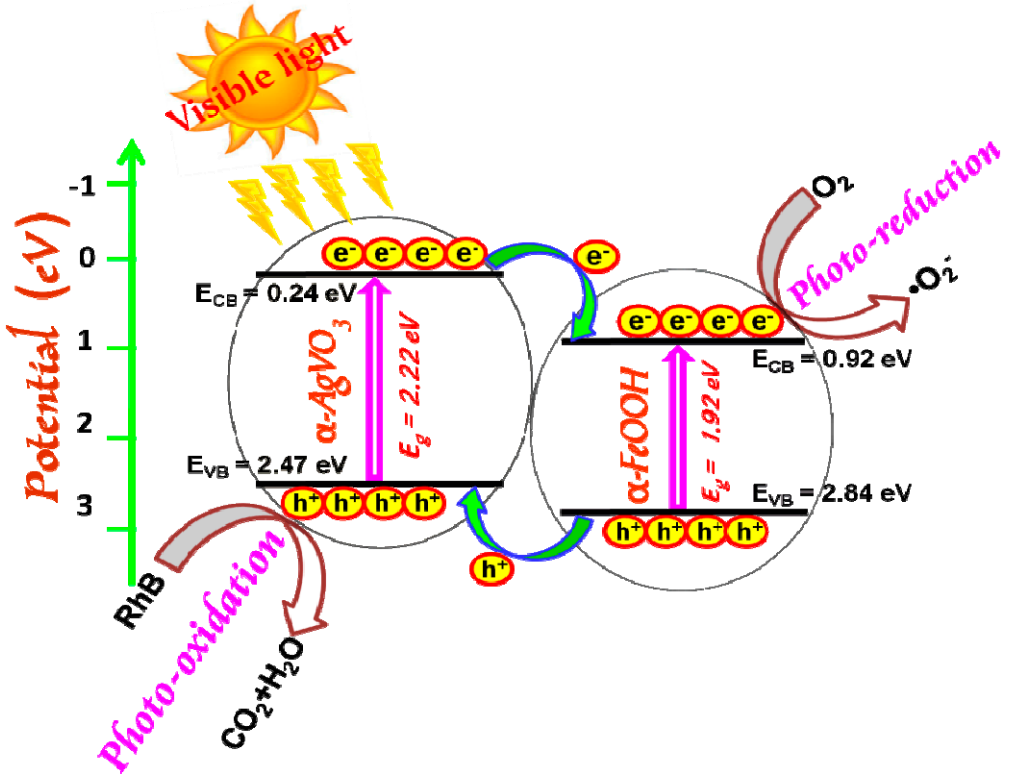

Figure 10. A proposed charge-transfer mechanism for the increased degradation of RhB using α-FeOOH/α-$AgVO_3$ nanocomposite photocatalysts under visible-light illumination.

3. Materials and Methods

3.1. Materials

Silver nitrate ($AgNO_3$) was purchased from Shantou Xilong Chemical (Guangdong, China). Ammonium metavanadate (NH_4VO_3) was obtained from Tianjin Guangfu Fine chemical (Tianjin China). Iron nitrate nonahydrate ($Fe(NO_3)_3 \bullet 9H_2O$) and ammonium oxalate (AO) were purchased from Tianjin Fuchen Chemical Reagent Co., Ltd. (Tianjin, China). Isopropyl alcohol (IPA), Benzoquinone (BQ) and absolute ethanol were bought from Beijing Chemical Industry Co., Ltd (Beijing, China). Rhodamine B (RhB) was received from Tianjin Hengxing Chemical Factory (Tianjin, China). All the above chemicals and reagents were of analytical grade and used without any further purification.

3.2. Synthesis of α-FeOOH Nanorods

The pure α-FeOOH nanorods were synthesized via a simple solvothermal method. Briefly, 1 g of $Fe(NO_3)_3 \bullet 9H_2O$ was dissolved in 30 mL of isopropanol and 30 mL of deionized (DI) water by magnetically stirring for 30 m at room temperature. The reaction solution pH was adjusted to 12.0 using 0.5 M NaOH solution, and the solution was stirred again for 30 min. Then, the obtained mixture was moved into a 100 mL Teflon-lined stainless steel autoclave followed by the solvothermal reaction carried out at 180 °C for 12 h. Lastly, the acquired precipitate was filtered and washed with DI water and absolute ethanol several times to wash out all the impurities if any and then dried at 80 °C for 3 h.

3.3. Synthesis of α-FeOOH/α-$AgVO_3$ Nanocomposites

The rod-on-rod–like α-FeOOH/α-$AgVO_3$ nanocomposite photocatalysts were synthesized by a facile co-precipitation method. First, the different amounts of (1 mg, 2 mg, 3 mg, 4 mg and 5 mg) of α-FeOOH nanorods and 2 mmol of $AgNO_3$ were dissolved in a beaker using 30 mL of DI water by ultra-sonication. At the same time, 2 mmol of NH_4VO_3 was dissolved in another beaker using 30 mL of DI water by ultra-sonication. Then, the NH_4VO_3 solution was slowly dripped into the α-FeOOH-$AgNO_3$ containing solution under stirring. After the addition of NH_4VO_3 the solution, the formed precipitate was continuously stirred for 3 h in indoor light-shielding conditions. Finally, the attained α-FeOOH/α-$AgVO_3$ nanocomposites were filtered and washed with DI water and absolute ethanol regularly, several times to remove impurities if any and then dried at 80 °C for 3 h. For comparison, the pure α-$AgVO_3$ was also synthesized by the same method without adding α-FeOOH. Furthermore, the as-synthesized α-FeOOH/α-$AgVO_3$ nanocomposites with 1 mg, 2 mg, 3 mg, 4 mg and 5 mg α-FeOOH were denoted as FeAVO-1, FeAVO-2, FeAVO-3, FeAVO-4 and FeAVO-5, respectively in the present work.

3.4. Characterization Techniques

The as-synthesized α-FeOOH/α-$AgVO_3$ nanocomposite photocatalysts were characterized by using various techniques. The X-ray powder diffraction (XRD) patterns of the samples were collected by a Rigaku D/Max2500VB2+/PCX diffractometer with Cu Kα radiation in 2θ range from 10° to 80° at a scan rate of 10° min^{-1}. The Fourier transform infrared (FT-IR) spectra of the samples were completed via Perkin-Elmer FT-IR spectrometer in the range of 400 cm^{-1}–4000 cm^{-1}. The UV-Vis diffuse reflectance spectra of the samples were conducted on a Shimadzu UV-2600 (Tokyo, Japan) UV-vis spectrophotometer. The scanning electron microscopy (SEM) measurements of samples were performed on a Hitachi S-4700 scanning electron microscope at an accelerating voltage of 20 kV. The high-resolution transmission electron microscopy (HR-TEM) measurements of the samples were carried out by a H-800 JEOL JEM-2100F high-resolution transmission electron microscope operated at 300.0 kV. The X-ray photoelectron spectra (XPS) of the samples were performed on a Thermo Fisher ESCAESCALAB 250 X-ray photoelectron spectrometer with monochromated Al Kα radiation source.

3.5. Photocatalytic Degradation Experiments

The photocatalytic activities of the as-synthesized photocatalysts were evaluated towards the degradation of RhB under visible-light irradiation. The 500 W xenon lamp was used as a visible-light source which was connected with a UV light cut-off filter in order to cut wavelength below 420 nm. In each experiment, 50 mg of the photocatalyst was well dispersed in 50 mL RhB dye solution (1×10^{-5} M). Prior to irradiation, the suspension was magnetically stirred in the dark for 30 min to achieve adsorption-desorption equilibrium. During irradiation, 5 mL suspension was taken out after a proper time interval and centrifuged to eliminate the photocatalyst particles. Afterwards, the concentration of the RhB was measured via a MAPADA UV-visible spectrophotometer (Shanghai,

China) based on its characteristic absorbance (λ_{max}) at 554 nm. The degradation efficiency of the photocatalysts was calculated using Equation (4).

$$\text{Efficiency}(\%) = \frac{C_0 - C}{C_0} \times 100\% = \frac{A_0 - A}{A_0} \times 100\% \quad (4)$$

Here, C_0 and A_0 denotes the concentration and absorption of dye at the time t = 0, respectively, and C and A denotes the concentration and absorption of the dye at certain time intervals.

4. Conclusions

In conclusion, a series of α-FeOOH/α-$AgVO_3$ nanocomposite photocatalysts were synthesized by a facile co-precipitation method with the different contents of solvothermaly obtained α-FeOOH nanorods for the first time. The structural, morphological, optical natures and elemental compositions of the as-synthesized photocatalysts were investigated by XRD, FT-IR, DRS-UV, FE-SEM, elemental mapping, HR-TEM and XPS analysis. The photocatalytic activities of the α-FeOOH/α-$AgVO_3$ nanocomposites were evaluated by the degradation of RhB dye under visible-light excitation. It can be demonstrated that the α-FeOOH/α-$AgVO_3$ nanocomposite obtained from 3 mg of α-FeOOH displays a greater photocatalytic activity when compared with that of pure α-$AgVO_3$ and α-FeOOH. This observed efficient photocatalytic activity of the nanocomposite is mainly ascribed to the increased charge separation efficiency and high visible-light absorption ability. Meanwhile, this optimized α-FeOOH/α-$AgVO_3$ nanocomposite exhibits the outstanding photostability and reusability properties. An acceptable charge-transfer mechanism for the enhanced degradation of RhB over α-FeOOH/α-$AgVO_3$ nanocomposite has also been proposed. Thereby, the above acquired results revealed that the α-FeOOH/α-$AgVO_3$ nanocomposite can be a prospective degradation material for application in wastewater treatment.

Author Contributions: J.P. proposed the concept, and supervised the research work at BUCT. M.S., R.A.S. and J.P. designed the experiments; M.S., R.A.S., S.O. and A.K. performed the experiments. All authors analyzed the data and wrote the paper.

Funding: This research was funded by the National Natural Science Foundation of China grant number (21676022), and the Fundamental Research Funds for the Central Universities grant number (BHYC1701A & JD1701).

Conflicts of Interest: The authors declare no conflicts of interest.

References

1. Ameta, R.; Benjamin, S.; Ameta, A.; Ameta, S.C. Photocatalytic Degradation of Organic Pollutants: A Review. *Mater. Sci. Forum* **2013**, *734*, 247–272. [CrossRef]
2. Delsouz Khaki, M.R.; Shafeeyan, M.S.; Abdul Raman, A.A.; Wan Daud, W.M.A. Application of doped photocatalysts for organic pollutant degradation: A review. *J. Environ. Manag.* **2017**, *198*, 78–94. [CrossRef] [PubMed]
3. Theerthagiri, J.; Murthy, A.P.; Elakkiya, V.; Chandrasekaran, S.; Nithyadharseni, P.; Khan, Z.; Senthil, R.A.; Shanker, R.; Raghavender, M.; Kuppusami, P.; et al. Recent development on carbon based heterostructures for their applications in energy and environment: A review. *J. Ind. Eng. Chem.* **2018**, *64*, 16–59.
4. Bora, L.V.; Mewada, R.K. Visible/solar light active photocatalysts for organic effluent treatment: Fundamentals, mechanisms and parametric review. *Renew. Sustain. Energy. Rev.* **2017**, *76*, 1393–1421. [CrossRef]
5. Nadraha, P.; Gaberscek, M.; SeverSkapin, A. Selective degradation of model pollutants in the presence of core@shell TiO_2@SiO_2 photocatalyst. *Appl. Surf. Sci.* **2017**, *405*, 389–394. [CrossRef]
6. Teh, C.M.; Mohamed, A.R. Roles of titanium dioxide and ion-doped titanium dioxide on photocatalytic degradation of organic pollutants (phenolic compounds and dyes) in aqueous solutions: A review. *J. Alloys Compd.* **2011**, *509*, 1648–1660. [CrossRef]

7. Vinoth Kumar, J.; Karthik, R.; Chen, S.M.; Muthuraj, V.; Karuppiah, C. Fabrication of potato-like silver molybdate microstructures for photocatalytic degradation of chronic toxicity ciprofloxacin and highly selective electrochemical detection of H_2O_2. *Sci. Rep.* **2015**, *6*, 34149. [CrossRef] [PubMed]
8. Tan, Y.Y.; Guo, Y.; Gu, X.Y.; Gu, C. Effects of metal cations and fulvic acid on the adsorption of ciprofloxacin onto goethite. *Environ. Sci. Pollut. Res.* **2015**, *22*, 609–617. [CrossRef] [PubMed]
9. De Bel, E.; Dewulf, J.; Van Lagenhove, H.; Janssen, C. Influence of pH on the sonolysis of ciprofloxacin: Biodegradability, ecotoxicity and antibiotic activity of its degradation products. *Chemosphere* **2009**, *77*, 291–295. [CrossRef] [PubMed]
10. Wang, P.; He, Y.L.; Huang, C.H. Oxidation of fluoroquinolone antibiotics and structurally related amines by chlorine dioxide: Reaction kinetics, product and pathway evaluation. *Water Res.* **2010**, *44*, 5989–5998. [CrossRef] [PubMed]
11. De Lima Perini, J.A.; Perez-Moya, M.; Nogueira, R.F.P. Photo-Fenton degradation kinetics of low ciprofloxacin concentration using different iron sources and pH. *J. Photochem. Photobiol. A* **2013**, *259*, 53–58. [CrossRef]
12. Theerthagiri, J.; Senthil, R.A.; Priya, A.; Madhavan, J.; Michael, R.J.V.; Ashok kumar, M. Photocatalytic and photoelectrochemical studies of visible-light active α-Fe_2O_3-g-C_3N_4 nanocomposites. *RSC Adv.* **2014**, *4*, 38222–38229. [CrossRef]
13. Chang, Y.; Yu, K.; Zhang, C.; Li, R.; Zhao, P.; Lou, L.L.; Liu, S. Three-dimensionally ordered macroporous WO3 supported Ag_3PO_4 with enhanced photocatalytic activity and durability. *Appl. Catal. B Environ.* **2015**, *176–177*, 363–373. [CrossRef]
14. Sui, M.; Xing, S.; Sheng, L.; Huang, S.; Guo, H. Heterogeneous catalytic ozonation of ciprofloxacin in water with carbon nanotube supported manganese oxides as catalyst. *J. Hazard. Mater.* **2012**, *227–228*, 227–236. [CrossRef] [PubMed]
15. Sharma, M.; Behl, K.; Nigam, S.; Joshi, M. TiO_2-GO nanocomposite for photocatalysis and environmental applications: A green synthesis approach. *Vacuum* **2018**, *156*, 434–439. [CrossRef]
16. Pica, M.; Nocchetti, M.; Ridolfi, B.; Donnadio, A.; Costantino, F.; Gentili, P.L.; Casciola, M. Nanosized zirconium phosphate/AgCl composite materials: A new synergy for an efficient photocatalytic degradation of organic dye pollutants. *J. Mater. Chem. A* **2015**, *3*, 5525–5534. [CrossRef]
17. Theerthagiri, J.; Senthil, R.A.; Priya, A.; Madhavan, J.; Ashokkumar, M. Synthesis of a visible-light active V_2O_5-g-C_3N_4 heterojunction as an efficient photocatalytic and photoelectrochemical material. *New J. Chem.* **2015**, *39*, 1367–1374.
18. Yosefi, L.; Haghighi, M.; Allahyari, S. Solvothermal synthesis of flowerlike p-BiOI/n-$ZnFe_2O_4$ with enhanced visible light driven nanophotocatalyst used in removal of acid orange 7 from wastewater. *Sep. Purif. Technol.* **2017**, *178*, 18–28. [CrossRef]
19. Liu, Y.; Ding, S.; Xu, J.; Zhang, H.; Yang, S.; Duan, X.; Sun, H.; Wang, S. Preparation of a p-n heterojunction $BiFeO_3$@TiO_2 photocatalyst with a core-shell structure for visible-light photocatalytic degradation. *Chin. J. Catal.* **2017**, *38*, 1052–1062. [CrossRef]
20. Ong, C.B.; Ng, L.Y.; Mohammad, A.W. A review of ZnO nanoparticles as solar photocatalysts: Synthesis, mechanisms and applications. *Renew. Sustain. Energy Rev.* **2018**, *81*, 536–551. [CrossRef]
21. Wang, H.; Zhou, P.; Guo, R.; Wang, Y.; Zhan, H.; Yuan, Y. Synthesis of rectorite/Fe_3O_4/ZnO composites and their application for the removal of methylene blue dye. *Catalysts* **2018**, *8*, 107. [CrossRef]
22. Ren, H.-T.; Yang, Q. Fabrication of Ag_2O/TiO_2 with enhanced photocatalytic performances for dye pollutants degradation by a pH-induced method. *Appl. Surf. Sci.* **2017**, *396*, 530–538. [CrossRef]
23. Wang, X.; Ni, Q.; Zeng, D.; Liao, G.; Wen, Y.; Shan, B.; Xie, C. BiOCl/TiO_2 heterojunction network with high energy facet exposed for highly efficient photocatalytic degradation of benzene. *Appl. Surf. Sci.* **2017**, *396*, 590–598. [CrossRef]
24. Senthil, R.A.; Theerthagiri, J.; Selvi, A.; Madhavan, J. Synthesis and characterization of low-cost g-C_3N_4/TiO_2 composite with enhanced photocatalytic performanceunder visible-light irradiation. *Opt. Mater.* **2017**, *64*, 533–539. [CrossRef]
25. Xu, D.; Cheng, B.; Zhang, J.; Wang, W.; Yu, J.; Ho, W. Photocatalytic activity of Ag_2MO_4 (M=Cr, Mo, W) photocatalysts. *J. Mater. Chem. A* **2015**, *3*, 20153–20166. [CrossRef]
26. Li, Y.; Li, Y.; Ma, S.; Wang, P.; Hou, Q.; Han, J.; Zhan, S. Efficient water disinfection with Ag_2WO_4-doped mesoporous g-C_3N_4 under visible light. *J. Hazard. Mater.* **2017**, *338*, 33–46. [CrossRef] [PubMed]

27. Zhao, X.; Song, L.; Zhang, S. Synthesis of $AgCl/Ag_3PO_4$ composite photocatalysts and study on photodegradation activity based on a continuous reactor. *Photochem. Photobiol.* **2018**, *94*, 484–490. [CrossRef] [PubMed]
28. Chen, Z.; Wang, W.; Zhang, Z.; Fang, X. High-efficiency visible-light-driven Ag_3PO_4/AgI photocatalysts: Z-scheme photocatalytic mechanism for their enhanced photocatalytic activity. *J. Phys. Chem. C* **2013**, *117*, 19346–19352. [CrossRef]
29. Xu, Y.; Jing, L.; Chen, X.; Ji, H.; Xu, H.; Li, H.; Li, H.; Zhang, Q. Novel visible-light-driven Fe_2O_3/Ag_3VO_4 composite with enhanced photocatalytic activity toward organic pollutants degradation. *RSC Adv.* **2016**, *6*, 3600–3607. [CrossRef]
30. Zhang, X.; Zhang, J.; Yu, J.; Zhang, Y.; Cui, Z.; Sun, Y.; Hou, B. Fabrication of $InVO_4/AgVO_3$ heterojunctions with enhanced photocatalytic antifouling efficiency under visible-light. *Appl. Catal. B Environ.* **2018**, *220*, 57–66. [CrossRef]
31. Jin, J.; Liang, Q.; Song, Y.; Xu, S.; Li, Z.; Yao, C. Hydrothermal synthesis of g-C3N4/Ag_2MoO_4 nanocomposites for improved visible light photocatalytic performance. *J. Alloys Compd.* **2017**, *726*, 221–229. [CrossRef]
32. Li, W.; Chen, J.; Guo, R.; Wu, J.; Zhou, X.; Luo, J. Facile fabrication of a direct Z-scheme MoO_3/Ag_2CrO_4 composite photocatalyst with improved visible light photocatalytic performance. *J. Mater. Sci. Mater. Electron.* **2017**, *28*, 15967–15979. [CrossRef]
33. Luo, J.; Zhou, X.; Ning, X.; Zhan, L.; Ma, L.; Xu, X.; Huang, Z.; Liang, J. Synthesis and characterization of Z-scheme In_2S_3/Ag_2CrO_4 composites with an enhanced visible-light photocatalytic performance. *New J. Chem.* **2017**, *41*, 845–856. [CrossRef]
34. Ju, P.; Fan, H.; Zhang, B.; Shang, K.; Liu, T.; Ai, S.; Zhang, D. Enhanced photocatalytic activity of β-$AgVO_3$ nanowires loaded with Ag nanoparticles under visible light irradiation. *Sep. Purif. Technol.* **2013**, *109*, 107–110. [CrossRef]
35. Zhao, W.; Guo, Y.; Faiz, Y.; Yuan, W.T.; Sun, C.; Wang, S.M.; Deng, Y.H.; Zhuang, Y.; Li, Y.; Wang, X.M.; et al. Facile in-suit synthesis of $Ag/AgVO_3$ one-dimensional hybrid nanoribbons with enhanced performance of plasmonic visible-light photocatalysis. *Appl. Catal. B Environ.* **2015**, *163*, 288–297. [CrossRef]
36. Sivakumar, V.; Suresh, R.; Giribabu, K.; Narayanan, V. $AgVO_3$ nanorods: Synthesis, characterization and visible light photocatalytic activity. *Solid State Sci.* **2015**, *39*, 34–39. [CrossRef]
37. Singh, A.; Dutta, D.P.; Ballal, A.; Tyagi, A.K.; Fulekar, M.H. Visible light driven photocatalysis and antibacterial activity of $AgVO_3$ and $Ag/AgVO_3$ nanowires. *Mater. Res. Bull.* **2014**, *51*, 447–454. [CrossRef]
38. Lu, H.; Wang, J.; Du, Z.; Liu, Y.; Li, M.; Chen, P.; Zhang, L. In-situ anion-exchange synthesis $AgCl/AgVO_3$ hybrid nanoribbons with highly photocatalytic activity. *Mater. Lett.* **2015**, *157*, 231–234. [CrossRef]
39. Lin, X.; Guo, X.; Shi, W.; Guo, F.; Zhai, H.; Yan, Y.; Wang, Q. Ag_3PO_4 quantum dots sensitized $AgVO_3$ nanowires: A novel $Ag_3PO_4/AgVO_3$ nanojunction with enhanced visible-light photocatalytic activity. *Catal. Commun.* **2015**, *66*, 67–72. [CrossRef]
40. Wang, R.; Cao, L. Facile synthesis of a novel visible-light-driven $AgVO_3/BiVO_4$ heterojunction photocatalyst and mechanism insight. *J. Alloys Compd.* **2017**, *722*, 445–451. [CrossRef]
41. Yang, Y.; Liu, Y.; Huang, B.; Zhang, R.; Dai, Y.; Qin, X.; Zhang, X. Enhanced visible photocatalytic activity of a BiVO4@β-$AgVO_3$ composite synthesized by an in situ growth method. *RSC Adv.* **2014**, *4*, 20058–20061. [CrossRef]
42. Cao, L. Novel MoS_2-modified $AgVO_3$ composites with remarkably enhanced photocatalytic activity under visible-light irradiation. *Mater. Lett.* **2017**, *188*, 252–256. [CrossRef]
43. Lei, Z.; Wang, J.; Wang, L.; Yang, X.; Xu, G.; Tang, L. Efficient photocatalytic degradation of ibuprofen in aqueous solution using novel visible-light responsive graphene quantum dot/$AgVO_3$ nanoribbons. *J. Hazard. Mater.* **2016**, *312*, 298–306. [CrossRef] [PubMed]
44. Zhao, W.; Guo, Y.; Wang, S.; He, H.; Sun, C.; Yang, S. A novel ternary plasmonic photocatalyst: Ultrathin g-C_3N_4 nanosheet hybrided by $Ag/AgVO_3$ nanoribbons with enhanced visible-light photocatalytic performance. *Appl. Catal. B Environ.* **2015**, *165*, 335–343. [CrossRef]
45. Zhao, W.; Wei, Z.; Hea, H.; Xu, J.; Li, J.; Yang, S.; Sun, C. Supporting 1-D $AgVO_3$ nanoribbons on single layer 2-D graphitic carbon nitride ultrathin nanosheets and their excellent photocatalytic activities. *Appl. Catal. A Gen.* **2015**, *501*, 74–82. [CrossRef]
46. Ouyang, Q.; Li, Z.; Liu, J. Synthesis of β-$AgVO_3$ nanowires decorated with Ag_2CrO_4 with improved visible light photocatalytic performance. *Semicond. Sci. Technol.* **2018**, *33*, 055010. [CrossRef]

47. Wang, K.; Wu, X.; Zhang, G.; Li, J.; Li, Y. $Ba_5Ta_4O_{15}$ nanosheet/$AgVO_3$ nanoribbon heterojunctions with enhanced photocatalytic oxidation performance: Hole dominated charge transfer path and plasmonic effect insight. *ACS Sustain. Chem. Eng.* **2018**, *6*, 6682–6692. [CrossRef]
48. Padhi, D.K.; Parida, K. Facile fabrication of α-FeOOH nanorod/RGO composite: A robust photocatalyst for reduction of Cr (VI) under visible light irradiation. *J. Mater. Chem. A* **2014**, *2*, 10300–10312. [CrossRef]
49. Zhang, G.; Wang, Q.; Zhang, W.; Li, T.; Yuan, Y.; Wang, P. Effects of organic acids and initial solution pH on photocatalytic degradation of bisphenol A (BPA) in a photo-Fenton-like process using goethite (α-FeOOH). *Photochem. Photobiol. Sci.* **2016**, *15*, 1046–1053. [CrossRef] [PubMed]
50. Ghadim, A.R.A.; Alizadeh, S.; Khodam, F.; Rezvani, Z. Synthesis of rod-like α-FeOOH nanoparticles and its photocatalytic activity in degradation of an azo dye: Empirical kinetic model development. *J. Mol. Catal. A Chem.* **2015**, *408*, 60–68. [CrossRef]
51. Li, Y.; Zhang, F.S. Catalytic oxidation of methyl orange by an amorphous FeOOH catalyst developed from a high iron-containing fly ash. *Chem. Eng. J.* **2010**, *158*, 148–153. [CrossRef]
52. Malathi, A.; Arunachalam, P.; Madhavan, J.; Al-Mayouf, A.M.; Ghanem, M.A. Rod-on-flake α-FeOOH/BiOI nanocomposite: Facile synthesis, characterization and enhanced photocatalytic performance. *Coll. Surf. A Physicochem. Eng. Asp.* **2018**, *537*, 435–445. [CrossRef]
53. Zhang, W.; Hu, C.; Tan, J.; Fan, Z.; Sun, Y.; Ran, S.; Chi, F.; Liu, X.; Lv, Y. Novel α-FeOOH nanorods/Ag_3PO_4 semiconductor composites with enhanced photocatalytic activity and stability. *Nano* **2016**, *11*, 1650071. [CrossRef]
54. Yang, H.; Zhang, S.; Cao, R.; Deng, X.; Li, Z.; Xu, X. Constructing the novel ultrafne amorphous iron oxyhydroxide/g-C_3N_4 nanosheets heterojunctions for highly improved photocatalytic performance. *Sci. Rep.* **2017**, *7*, 8686. [CrossRef] [PubMed]
55. McNulty, D.; Ramasse, Q.; ODwyer, C. The structural conversion from α-$AgVO_3$ to β-$AgVO_3$: Ag nanoparticle decorated nanowires with application as cathode materials for Li-ion batteries. *Nanoscale* **2016**, *8*, 16266–16275. [CrossRef] [PubMed]
56. De Castro, D.T.; Valente, M.L.C.; Da Silva, C.H.L.; Watanabea, E.; Siqueira, R.L.; Schiavon, M.A.; Alves, O.L.; Dos Reis, A.C. Evaluation of antibiofilm and mechanical properties of new nanocomposites based on acrylic resins and silver vanadate nanoparticles. *Arch. Oral Biol.* **2016**, *67*, 46–53. [CrossRef] [PubMed]
57. Li, J.; Yu, C.; Fang, W.; Zhu, L.; Zhou, W.; Fan, Q. Preparation, characterization and photocatalytic performance of heterostructured AgCl/Bi_2WO_6 microspheres. *Chin. J. Catal.* **2015**, *36*, 987–993. [CrossRef]
58. Zhang, W.; Zhou, L.; Shi, J.; Deng, H. Synthesis of Ag_3PO_4/G-C_3N_4 composite with enhanced photocatalytic performance for the photodegradation of diclofenac under visible light irradiation. *Catalyst* **2018**, *8*, 45. [CrossRef]
59. Kiantazh, F.; Yangjeh, A.H. Ag_3VO_4/ZnO nanocomposites with an n-n heterojunction as novel visible-light-driven photocatalysts with highly enhanced activity. *Mater. Sci. Semicond. Proc.* **2015**, *39*, 671–679. [CrossRef]
60. Qiu, F.; Zhu, X.; Guo, Q.; Dai, Y.; Xu, J.; Zhang, T. Fabrication of a novel hierarchical flower-like hollow structure Ag_2WO_4/WO_3 photocatalyst and its enhanced visible-light photocatalytic activity. *Powder Technol.* **2017**, *317*, 287–292. [CrossRef]
61. Senthil, R.A.; Priya, A.; Theerthagiri, J.; Selvi, A.; Nithyadharseni, P.; Madhavan, J. Facile synthesis of α-Fe_2O_3/WO_3 composite with an enhanced photocatalytic and photo-electrochemical performance. *Ionics* **2018**. [CrossRef]

© 2018 by the authors. Licensee MDPI, Basel, Switzerland. This article is an open access article distributed under the terms and conditions of the Creative Commons Attribution (CC BY) license (http://creativecommons.org/licenses/by/4.0/).